Sensors & Diagnostics

PAPER

View Article Online
View Journal | View Issue

Cite this: *Sens. Diagn.*, 2022, **1**, 1218

Polymer dots synergized with a NiO hole transporting layer and poly(amido amine) dendrimer: toward sensitive photocathodic detection of tyrosinase level in serum†

Jia-Hao Chen,[abd] Cheng-Shuang Wang,*[ad] Yu-Yue Zhu,[d] Cheng-Jie Li,[d] Cheng-Jun Li,[d] Fen-Ying Kong, *[c] Wei-Wei Zhao, *[d] Jing-Juan Xu [d] and Hong-Yuan Chen[d]

Received 26th July 2022,
Accepted 1st September 2022

DOI: 10.1039/d2sd00131d

rsc.li/sensors

The tyrosinase (TYR) level in human serum has been generally regarded as a biomarker of metastatic melanoma and vitiligo. In this work, established upon a unique poly(amido amine) (PAMAM)/polymer dots (Pdots)/NiO hole transporting layer (HTL) heterostructure, cathodic photoelectrochemical bioanalysis has been demonstrated for TYR detection in serum. In the detection, TYR could catalyze the generation of electron acceptor quinones, which could be covalently coupled to the amine groups on the PAMAM through the Michael addition reaction. The photo-induced electron transfer (PET) from Pdots/NiO heterojunction to quinones under light stimulation would result in high-efficacy generation of cathodic photocurrents, and the as-prepared photocathodic biosensor could achieve sensitive TYR detection in a linear range of 0.1–1000 U L^{-1} (R^2 = 0.996) with a detection limit of 0.03 U L^{-1}. The biosensor also exhibits applicability to TYR in actual human serum samples. This work provides a feasible platform for photocathodic bioanalysis towards TYR detection, which is envisioned to be applied for practical clinical diagnosis.

Introduction

Tyrosinase (TYR), a copper-containing polyphenol oxidase enzyme in plants, animals and the human body, is essential for melanogenesis and pigmentation.[1] It can catalyze the *ortho*-hydroxylation of phenol derivatives and further oxidation to form quinone products under oxygen. As the only human melanogenic enzyme with a well-established *in vivo* catalytic activity,[2] TYR widely exists in highly specialized melanocytes in the skin, hair bulbs, and eyes that produce pigment. In clinical research, the TYR level in the human serum helps identify the incubated metastatic melanoma and vitiligo and is closely correlated with the pathogenesis of Parkinson's disease.[3] Quantitative detection of TYR is thus essential and currently being developed with technologies including colorimetry,[4] Raman scattering,[5] electrochemistry,[6] electrochemiluminescence[7] and fluorescence method.[8–10] While each of the techniques has specific merits, they also suffer from disadvantages like high cost and low sensitivity.

Photoelectrochemical (PEC) bioanalysis is a rapidly developing methodology for sensitive biomolecule detection with a fast response, low background and high sensitivity.[11–16] In comparison with the well-studied photoanodic bioanalysis,[17–26] serious consideration of p-type light-harvesting materials for photocathodic bioanalysis is relatively recent.[27–31] Nevertheless, because of their desirable properties such as higher stability than the anodic system and superior anti-interference capability against reductive substances in actual biological samples, exploration in this direction is gaining strong momentum.[32] Bearing in mind the advantages of photocathodic bioanalysis and the significance of TYR, it is of particular interest to accomplish innovative photocathodic bioanalysis of TYR.

Semiconducting conjugated polymer dots (Pdots) represent a family of functional nanomaterials with readily

[a] *School of Materials Science and Engineering, Yancheng Institute of Technology, Yancheng, 224051, China. E-mail: wcsycit@163.com*
[b] *School of Mechanical Engineering, Yancheng Institute of Technology, Yancheng 224051, China*
[c] *School of Chemistry and Chemical Engineering, Yancheng Institute of Technology, Yancheng 224051, China. E-mail: kongfy@ycit.edu.cn*
[d] *State Key Laboratory of Analytical Chemistry for Life Science, School of Chemistry and Chemical Engineering, Nanjing University, Nanjing, 210023, China. E-mail: zww@nju.edu.cn*

† Electronic supplementary information (ESI) available. See DOI: https://doi.org/10.1039/d2sd00131d

modulated electrical and optical properties, easy synthesis, low cytotoxicity, high biocompatibility, and excellent photostability.[33] Previously, we and others explored the PEC properties of Pdots and applied Pdots toward the PEC detection of L-cysteine,[34] pH,[35] DNA,[36] miRNA-141,[37] telomerase activity,[38] sialic acid,[39] α-solanine,[40] *etc.* Despite the desirable potential, the study of Pdots for advanced PEC bioanalysis is still in its infancy.

Hierarchical semiconducting heterostructures integrating different properties of the individual components could improve the hybrid performances. The hole transporting layer (HTL) is a layer that has high hole mobility and affinity. As a critical component of the photoactive electrode, it could significantly impact the photoelectrode's photoelectron conversion efficiency and stability. Small bandgap Pdots integrated with a proper bandgap HTL are expected to present a novel p–p heterostructure with strengthened charge extraction and transporting efficiencies.[32] Among various HTLs, nickel oxide (NiO) was widely utilized as an HTL in solar energy devices, where light absorption in a photoactive layer is followed by charge separation and hole injection into the NiO HTL.[41,42] However, the possibility of constructing Pdots/HTL, *e.g.*, Pdots/NiO HTL, and their application for photocathodic bioanalysis has not been unveiled.

Poly(amido amine) (PAMAM) dendrimers are hyperbranched polymers with numerous active amine groups on the terminal surface. Their structural versatility facilitates the conjugation of various targeting ligands and has been used for drug delivery, cancer targeting, and imaging. PAMAM dendrimers could also be used as crosslinkers or building blocks to construct various crosslinked networks. In the field of biomolecular detection, dendrimer-involved biosensors using building blocks of PAMAM dendrimers have also been reported.[43] Given their structural properties and numerous amine groups, their innovative application in PEC bioanalysis is highly expected.

Herein, this work reported the development of a PAMAM/Pdots/NiO HTL electrode for sensitive photocathodic detection of TYR in human serum. As illustrated in Fig. 1a, tetraphenylporphyrin (TPP)-doped poly[(9,9′-dioctylfluorenyl-2,7-diyl)-*co*-(1,4-benzo-{2,1′,3}-thiadiazole)] (PFBT) Pdots was synthesized *via* a reprecipitation technique with PFBT, photosensitizer TPP and poly(styrene-*co*-maleic anhydride). Meanwhile, as shown in Fig. 1b, the PAMAM/Pdots/NiO HTL electrode was prepared by liquid phase deposition and annealing treatment of NiO nanosheets on fluorine-doped tin oxide (FTO), and then by layer-by-layer assembly of Pdots, followed by covalent bonding with the PAMAM through the 1-ethyl-3-(3-dimethylaminopropyl) carbodiimide hydrochloride/*N*-hydroxysuccinimide (EDC/NHS)-involved amidation reaction between the carboxylic acids on the surface of the Pdots and the amine groups on PAMAM. In connection to TYR-enabled oxidization of hydroquinone to 1,4-benzoquinone (BQ) in the presence of oxygen (Fig. 1c), BQ would covalently attach to the amino groups of PAMAM through the Michael addition reaction. Upon illumination, the NiO HTL could efficiently accelerate the hole transfer from Pdots to the metal contact, with the simultaneous photo-induced electron transfer (PET) from Pdots to BQ as electron acceptors. Correlated with the TYR activity, the cathodic photocurrent of the PAMAM/Pdots/NiO/FTO could be remarkably enhanced with the increased BQ, thus allowing quantitative TYR detection. The biosensor also exhibits applicability to TYR in actual human serum samples. This work features the use of a unique PAMAM/Pdots/inorganic HTL electrode for sensitive photocathodic TYR detection, which has not been reported to our knowledge.

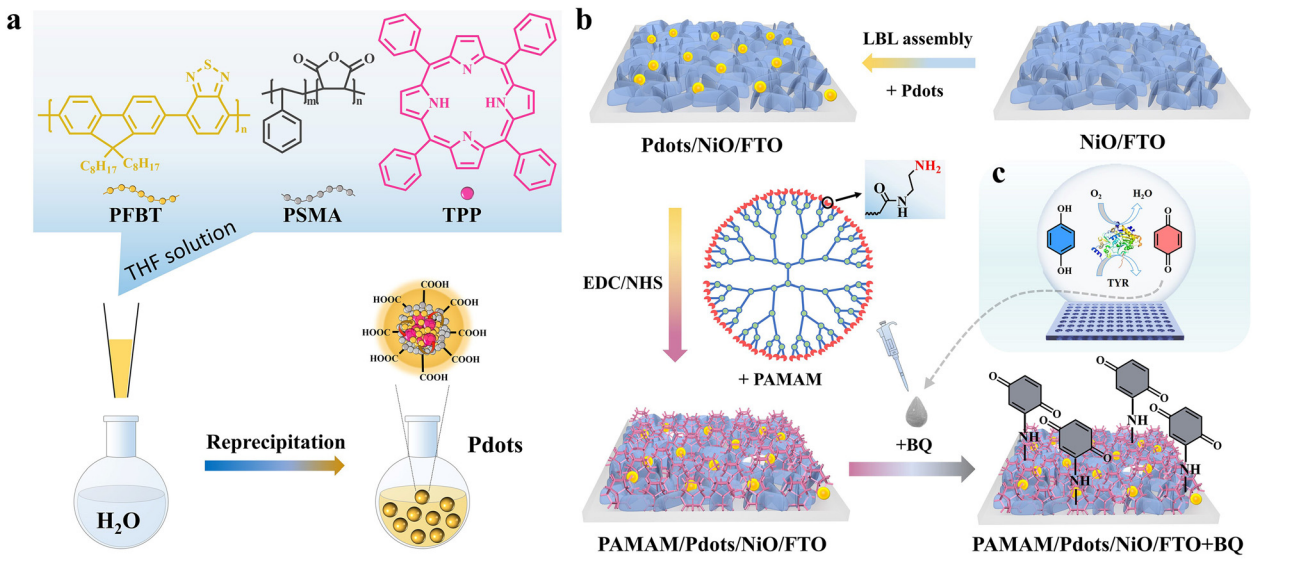

Fig. 1 (a) Schematic route to synthesize TPP-doped PFBT Pdots. (b) Schematic illustration of PAMAM/Pdots/NiO/FTO with covalently attached BQ. (c) Illustration of the TYR-enabled oxidization of hydroquinone to the BQ.

Experimental

Reagents and materials

The reagents used in the experiment were purchased from reagent companies. Human blood samples were collected from Yizheng People's Hospital affiliated with the Medical College of Yangzhou University. All experiments were performed under the Guidelines "Helsinki Declaration" and approved by the ethics committee at Yangzhou University. Informed consent was obtained from the human participants in this study. More information, such as synthesis, fabrication and characterization, is available in the ESI.†

PEC strategy for profiling TYR

A unique PAMAM/Pdots/NiO/FTO was exploited for sensitive photocathodic bioanalysis of TYR. Specifically, we prepared a TYR incubation solution containing 20 μL of 1 mM hydroquinone, 20 μL of different concentrations of TYR and 160 μL of 10 mM phosphate buffered saline (PBS, pH 7.4). The TYR reaction mixture was set in a 96-well plate for 2 h at 37 °C to allow BQ generation. Then, 20 μL of the reaction mixture was dropped on the PAMAM/Pdots/NiO/FTO for 10 min, and the electrode was carefully washed with 10 mM PBS. Finally, the PAMAM/Pdots/NiO/FTO was tested in 10 mM PBS at 0 V.

Results and discussion

Experimentally, the morphology and size of the as-fabricated Pdots were characterized by transmission electron microscopy (TEM). As shown in Fig. 2a, the Pdots appeared as quasi-spherical nanoparticles with diameters of ~2.8 nm. On the other hand, NiO as an HTL has advantages with good stability and high hole-transporting ability. The morphology of the NiO nanosheets was observed using scanning electron microscopy (SEM) and is illustrated in Fig. 2b. The NiO film displayed a highly crossed porous framework comprising densely interconnected nanosheets. As shown in the Fig. 2b inset, the cross-sectional view revealed that the height of the NiO nanosheet film was ~300 nm. The porous nanostructure has a high surface area, which is conducive to exchanging electrodes and electrolytes. The chemical composition of the NiO nanosheet film and Pdots/NiO/FTO was further characterized by X-ray photoelectron spectroscopy (XPS), as shown in Fig. S1.†

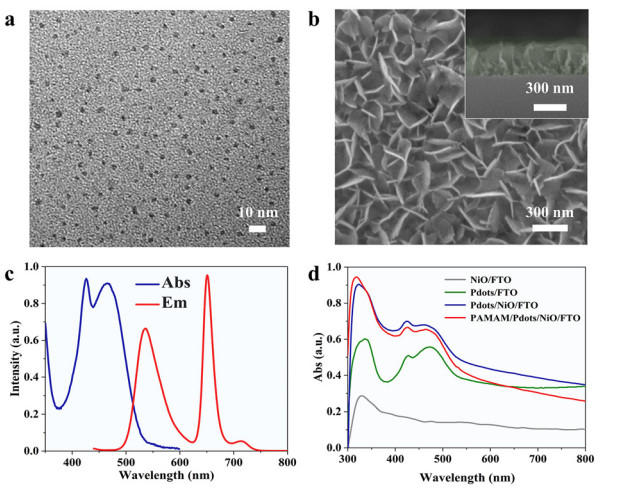

Fig. 2 (a) TEM image of the as-synthesized Pdots. (b) SEM images of the surface and the cross-sectional view of the NiO/FTO (inset). (c) Normalized absorption (blue) and emission (red) spectra of the Pdots. (d) UV-vis absorption spectra of the NiO/FTO (grey), Pdots/FTO (green), Pdots/NiO/FTO (blue) and PAMAM/Pdots/NiO/FTO (red).

To examine the light-harvesting and emitting properties of Pdots, we investigated the UV-vis absorption and fluorescence emission spectra of the Pdots. As shown in Fig. 2c, the absorption spectrum of PFBT Pdots with a 5 wt% TPP doping fraction exhibited two dominant adsorption peaks at 426 and 465 nm corresponding to the absorption of TPP molecules and PFBT, respectively.[33] The emission spectrum of Pdots shows red fluorescence at 650 nm of the TPP acceptors, with the fluorescence at 536 nm of PFBT being partly quenched. This was attributed to the PFBT absorption and transfer of the excitation energy to photosensitizer TPP molecules.[36] The Pdots/NiO/FTO heterojunction was fabricated and characterized by a UV-vis-NIR photospectrometer. As shown in Fig. 2d, the absorption of the Pdots/NiO/FTO was integrated into the NiO/FTO and Pdots/FTO spectra, which confirmed the layer-by-layer assembly of Pdots on the NiO/FTO. After PAMAM was covalently attached to the surface of Pdots/NiO/FTO, the absorption spectra of the resulting electrode exhibited almost no change in the 300–500 nm range.

To investigate the PEC properties of the photocathode, the chronoamperometric *I–t* curves were measured upon the 455 nm intermittent light irradiation. As shown in Fig. 3a, the NiO/FTO and Pdots/FTO exhibited a cathodic photocurrent of ~1.3 nA and ~35.6 nA, respectively. After forming the Pdots/NiO/FTO heterostructures, the cathodic photocurrent increased significantly up to 93.0 nA, which could be attributed to the good hole transfer efficiency of NiO HTL. The cathodic photocurrent of the PAMAM/Pdots/NiO/FTO slightly decreased to ~79.7 nA when PAMAM was covalently attached to the surface of Pdots/NiO/FTO, which was due to the steric effect of the dendrimers. Fig. 3b illustrates the charge transfer route of Pdots/NiO/FTO with well-matched energy levels. Upon light irradiation, the photoexcitation of Pdots led to separated electrons and holes on their LUMO and HOMO, the holes were spontaneously transported to the NiO HTL, because the HOMO energy level (1.2 V *vs.* normal hydrogen electrode (NHE))[44] of Pdots was more positive than the valence band potential (0.54 V *vs.* NHE)[45] of NiO. At the same time, the electrons in the LUMO (−1.14 V *vs.* NHE) of Pdots would rapidly transfer to BQ through a PET process. The stability of the photocurrent response of the PAMAM/Pdots/NiO/FTO was also evaluated, as shown in Fig. S2.† The as-fabricated

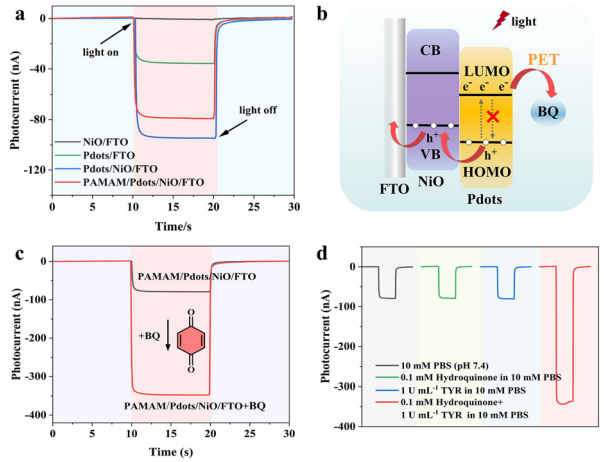

Fig. 3 (a) PEC response of the as-synthesized NiO/FTO (grey), Pdots/FTO (green), Pdots/NiO/FTO (blue) and PAMAM/Pdots/NiO/FTO (red) in 10 mM PBS. (b) The charge transfer route of illuminated Pdots/NiO/FTO. (c) PEC responses of the PAMAM/Pdots/NiO/FTO with 1 mM BQ. (d) PEC response of the PAMAM/Pdots/NiO/FTO in 10 mM PBS (grey), 0.1 mM hydroquinone in 10 mM PBS (green), 1 U mL^{-1} TYR in 10 mM PBS (blue), and the mixture of 0.1 mM hydroquinone and 1 U mL^{-1} TYR in 10 mM PBS (red).

electrode displayed reproducible responses without a noticeable change during 25 repeated on/off illumination cycles, indicating its good photophysical stability.

To validate the feasibility of PAMAM/Pdots/NiO/FTO toward photocathodic detection of TYR, the effect of covalently attached BQ was studied. As shown in Fig. 3c, the photocurrent of the PAMAM/Pdots/NiO/FTO significantly increased from 79.7 nA to 350.4 nA with 1 mM BQ, demonstrating that BQ could serve as the electron acceptor to improve the cathodic photocurrent. We further investigated the effect of hydroquinone on the photocurrent with or without TYR. As shown in Fig. 3d, the photocurrent of the PAMAM/Pdots/NiO/FTO did not change in different solutions, *e.g.*, 10 mM PBS, 0.1 mM hydroquinone or 1 U mL^{-1} TYR in 10 mM PBS. When mixing 0.1 mM hydroquinone as the substrate and 1 U mL^{-1} TYR in 10 mM PBS, the *in situ* generation of BQ through TYR catalyzed oxidation of hydroquinone could increase the photocurrent of PAMAM/Pdots/NiO/FTO. These results verified that BQ not only could be covalently attached to the surface of PAMAM/Pdots/NiO/FTO, but could also enhance the photocurrent response of the PAMAM/Pdots/NiO/FTO.

Toward the quantitative detection of TYR activity, we then investigated the PEC performance of PAMAM/Pdots/NiO/FTO with *in situ* enzyme-catalyzed generation of BQ. Fig. 4a shows the effect of different TYR concentrations on the photocurrent responses. Obviously, the photocurrent improved gradually with an increased TYR activity. As shown in Fig. 4b, the photocurrent enhancement $(I–I_0)/I_0$ was logarithmically related to the TYR concentration in the linear range of 0.1–1000 U L^{-1}, where the

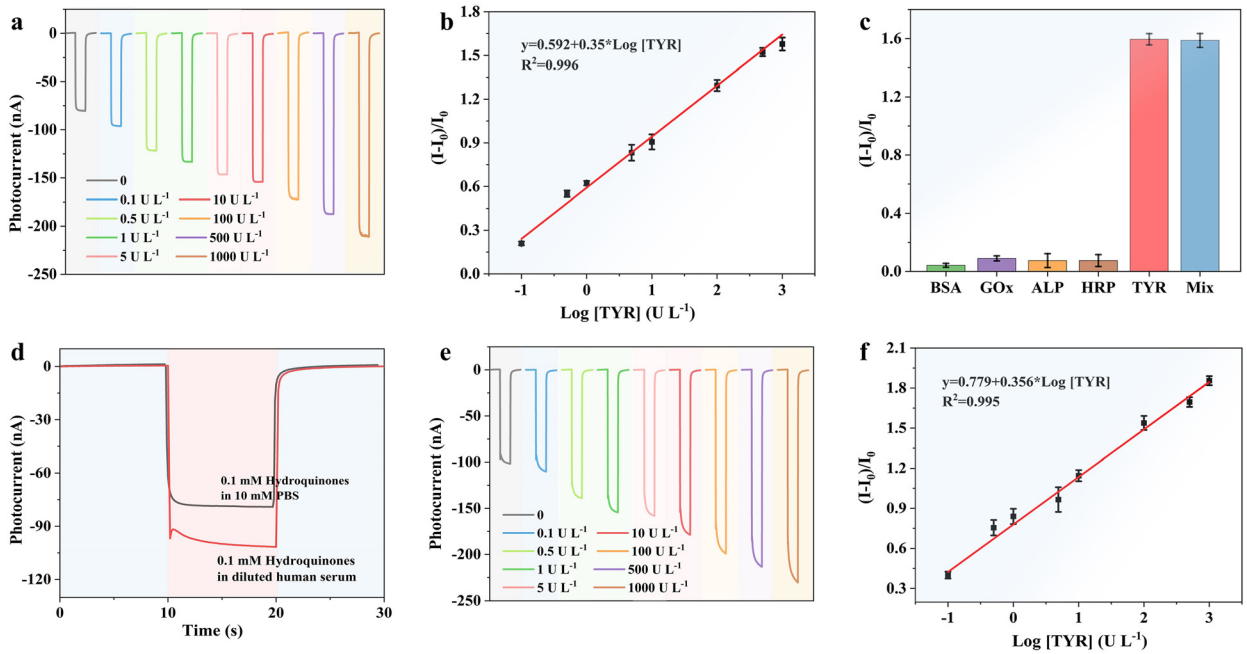

Fig. 4 (a) PEC response of the as-fabricated electrode in different TYR concentrations (0, 0.1, 0.5, 1, 5, 10, 100, 500, and 1000 U L^{-1}) containing 0.1 mM hydroquinone. (b) Calibration curve to TYR with varied concentrations. $(I–I_0)/I_0$ as a function of TYR concentration. I_0 was defined as the initial photocurrent, and I was defined as the photocurrent after the reaction. (c) Selectivity for TYR detection. The concentration of hydroquinone was 0.1 mM, and those for TYR, BSA, GOx, ALP and HRP were 1 U mL^{-1}. (d) PEC response of the as-fabricated electrode with 0.1 mM hydroquinone in the 10^4-fold diluted human serum. (e) PEC response of the as-fabricated electrode in different TYR concentrations (0, 0.1, 0.5, 1, 5, 10, 100, 500, and1000 U L^{-1}) containing 0.1 mM hydroquinone in the 10^4-fold diluted human serum. (f) The corresponding calibration curve to TYR in the 10^4-fold diluted human serum $(I–I_0)/I_0$ as a function of TYR concentration.

Table 1 Comparison of performance of different TYR biosensors

Analytical methods	Linear region (U L^{-1})	LOD (U L^{-1})	Ref.
Colorimetry (fluorometry)	20–1.5 × 10^3 (10–1 × 10^3)	20 (10)	4
Surface-enhanced Raman scattering (SERS)	100–1 × 10^5	70	5
Fluorometry	1 × 10^3–1 × 10^5	500	9
Fluorometry	0–2 × 10^5	340	10
Fluorometry	45–319.5	13.5	47
Photoelectrochemistry	0.3–5 × 10^3	0.1	45
Photoelectrochemistry	0.1–100	0.1	48
Photoelectrochemistry	50–1 × 10^4	16	49
Photoelectrochemistry	0.1–1000	0.03	This work

fitted linear equation could be described as $(I–I_0)/I_0$ = 0.592 + 0.35 × log[TYR] (R^2 = 0.996). The value of $(I–I_0)/I_0$ was 2% corresponding to pure PBS, and hence the lowest detection limit was calculated to be 0.03 U L^{-1} (S/N = 3). The detection limit of the biosensor was comparable to previous reports as listed in Table 1. The selectivity was investigated with different interferents including bovine serum albumin (BSA), glucose oxidases (GOx), alkaline phosphatase (ALP), horseradish peroxidase (HRP) and their mixtures. As shown in Fig. 4c, only TYR and the mixture could induce a significant photocurrent enhancement, indicating its good selectivity. To verify its potential for real applications, the TYR level in human serum samples was tested with a standard addition method. The TYR activity was detected in 10^4-fold diluted human serum with 10 mM PBS. Then different concentrations of TYR were injected into the diluted human serum samples.

As shown in Fig. 4d, the photocurrent significantly increased from 79.7 nA to 101.3 nA in diluted human serum. Based on the obtained linear equation, the concentration of TYR in the human serum was calculated to be 0.33 U mL^{-1}, which was consistent with the previously reported TYR activity of 0.1–1.2 U mL^{-1}.[46] Fig. 4e shows the effect of different TYR activities on the photocurrents, which improved consistently with increased TYR concentrations. As shown in Fig. 4f, the photocurrent enhancement $(I–I_0)/I_0$ was also logarithmically related to the TYR activities, and the fitted linear equation could be expressed as $(I–I_0)/I_0$ = 0.779 + 0.356 × log[TYR] (R^2 = 0.995). The corresponding linear curve demonstrated that this biosensor exhibited a similar sensitivity in PBS and actual biological samples.

Conclusion

In summary, this work reported the design of a unique PAMAM/Pdots/NiO electrode and its application toward photocathodic detection of the TYR activity in the real sample. NiO HTL could efficiently transfer the hole and enhance the charge separation of Pdots, whereas the numerous active amine groups of PAMAM could not only bind to –COOH on the Pdots but also covalently attached to BQ as electron acceptors. The as-developed PAMAM/Pdots/NiO HTL/FTO possessed high PEC stability, and its cathodic response correlated sensitively with the TYR activity. Due to the synergy effects of Pdots/NiO HTL and PAMAM, this biosensor exhibited good analytical performance in terms of high selectivity and sensitivity, with a linear range of 0.1–1000 U L^{-1} and a detection limit of 0.03 U L^{-1}. The actual applicability of this biosensor was also verified using real human serum. In addition to a promising TYR detection, we also envision that this work could stimulate more interest in the design and development of innovative biohybrid heterostructures for advanced photocathodic bioanalysis.

Author contributions

Jia-Hao Chen: methodology, data curation, investigation, and writing – original draft. Cheng-Shuang Wang: methodology, data curation, investigation, writing – review & editing, and funding acquisition. Yu-Yue Zhu: methodology and investigation. Cheng-Jie Li: methodology and investigation. Cheng-Jun Li: methodology and investigation. Fen-Ying Kong: writing – review & editing and project administration. Wei-Wei Zhao: conceptualization, writing – review & editing, and funding acquisition. Jing-Juan Xu: project administration. Hong-Yuan Chen: project administration.

Conflicts of interest

We declare that we have no conflict of interest.

Acknowledgements

This work was supported by the National Natural Science Foundation of China (Grant No. 51903217, 21974059, and 22174063).

References

1 Y. Teng, X. Jia, J. Li and E. Wang, *Anal. Chem.*, 2015, **87**, 4897–4902.
2 X. Wu, L. Li, W. Shi, Q. Gong and H. Ma, *Angew. Chem., Int. Ed.*, 2016, **55**, 14728–14732.
3 I. Carballo-Carbajal, A. Laguna, J. Romero-Gimenez, T. Cuadros, J. Bove, M. Martinez-Vicente, A. Parent, M. Gonzalez-Sepulveda, N. Penuelas, A. Torra, B. Rodriguez-Galvan, A. Ballabio, T. Hasegawa, A. Bortolozzi, E. Gelpi and M. Vila, *Nat. Commun.*, 2019, **10**, 973.
4 J. Zhao, G. Liu, J. Sun, Q. Wang, Z. J. Li and X. Yang, *Anal. Chem.*, 2020, **92**, 2316–2322.
5 L. Wang, Z. F. Gan, D. Guo, H. L. Xia, F. T. Patrice, M. E. Hafez and D. W. Li, *Anal. Chem.*, 2019, **91**, 6507–6513.
6 B. Ciui, A. Martin, R. K. Mishra, B. Brunetti, T. Nakagawa, T. J. Dawkins, M. Lyu, C. Cristea, R. Sandulescu and J. Wang, *Adv. Healthcare Mater.*, 2018, **7**, 1701264.
7 M. Liu, B. Zhang, M. Zhang, X. Hu, W. Chen, G. Fang and S. Wang, *Sens. Actuators, B*, 2020, **311**, 127901.
8 X. Yan, H. Li, W. Zheng and X. Su, *Anal. Chem.*, 2015, **87**, 8904–8909.

9 H. Li, W. Liu, F. Zhang, X. Zhu, L. Huang and H. Zhang, *Anal. Chem.*, 2018, **90**, 855–858.
10 Y. Cui, S. J. Park, X. Wu, R. Wang, S. Qi, H. M. Kim and J. Yoon, *Chem. Commun.*, 2021, **57**, 6911–6914.
11 W. W. Zhao, J. J. Xu and H. Y. Chen, *Chem. Rev.*, 2014, **114**, 7421–7441.
12 W. W. Zhao, J. J. Xu and H. Y. Chen, *Chem. Soc. Rev.*, 2015, **44**, 729–741.
13 M. J. Lu, F. Z. Chen, J. Hu, H. Zhou, G. Chen, X. D. Yu, R. Ban, P. Lin and W. W. Zhao, *Small Struct.*, 2021, **2**, 2100087.
14 Y. F. Ruan, F. Z. Chen, Y. T. Xu, T. Y. Zhang, S. Y. Yu, W. W. Zhao, D. Jiang, H. Y. Chen and J. J. Xu, *Angew. Chem., Int. Ed.*, 2021, **60**, 25762–25765.
15 J. Hu, M. J. Lu, F. Z. Chen, H. M. Jia, H. Zhou, K. Li, X. Zeng, W. W. Zhao and P. Lin, *Adv. Funct. Mater.*, 2022, **32**, 2109046.
16 Y. T. Xu, Z. Li, C. Yuan, J. Q. Wu, J. Hu, P. Lin, W. W. Zhao, H. Y. Chen and J. J. Xu, *Adv. Opt. Mater.*, 2022, **10**, 2102687.
17 W. W. Zhao, X. D. Yu, J. J. Xu and H. Y. Chen, *Nanoscale*, 2016, **8**, 17407–17414.
18 W. W. Zhao, J. J. Xu and H. Y. Chen, *Biosens. Bioelectron.*, 2017, **92**, 294–304.
19 J. Shu and D. Tang, *Anal. Chem.*, 2020, **92**, 363–377.
20 H. Zhou, J. Liu and S. Zhang, *TrAC, Trends Anal. Chem.*, 2015, **67**, 56–73.
21 Q. Cheng, J. Feng, T. Wu, N. Zhang, X. Wang, H. Ma, X. Sun and Q. Wei, *Anal. Chem.*, 2021, **93**, 13680–13686.
22 Z. Li, C. Su, D. Wu and Z. Zhang, *Anal. Chem.*, 2018, **90**, 961–967.
23 X. Tan, H. Yu, B. Liang, M. Han, S. Ge, L. Zhang, L. Li, L. Li and J. Yu, *Anal. Chem.*, 2022, **94**, 1705–1712.
24 Y. Fu, K. Zou, M. Liu, X. Zhang, C. Du and J. Chen, *Anal. Chem.*, 2020, **92**, 1189–1196.
25 X. Liu, Y. Zhao and F. Li, *Biosens. Bioelectron.*, 2021, **173**, 112832.
26 Z. Li, J. Hu, G. Gao, X. N. Liu, J. Q. Wu, Y. T. Xu, H. Zhou, W. W. Zhao, J. J. Xu and H. Y. Chen, *Sens. Diagn.*, 2022, **1**, 294–300.
27 Y. T. Xu, S. Y. Yu, Y. C. Zhu, G. C. Fan, D. M. Han, P. Qu and W. W. Zhao, *TrAC, Trends Anal. Chem.*, 2019, **114**, 81–88.
28 G. C. Fan, S. Gu, D. Zhang, Z. Hu and X. Luo, *Biosens. Bioelectron.*, 2020, **168**, 112563.
29 M. Qing, S. L. Chen, L. Han, Y. Z. Yang, H. Q. Luo and N. B. Li, *Biosens. Bioelectron.*, 2020, **158**, 112179.
30 H. M. Deng, M. J. Xiao, Y. Q. Chai, R. Yuan and Y. L. Yuan, *Biosens. Bioelectron.*, 2022, **197**, 113806.
31 H. Yang, J. Wang, H. Yu, X. Li, Z. Li, K. Cui, L. Zhang, S. Ge and J. Yu, *Chem. Eng. J.*, 2022, **430**, 132846.
32 X. Y. Jiang, L. Zhang, Y. L. Liu, X. D. Yu, Y. Y. Liang, P. Qu, W. W. Zhao, J. J. Xu and H. Y. Chen, *Biosens. Bioelectron.*, 2018, **107**, 230–236.
33 S. Li, K. Chang, K. Sun, Y. Tang, N. Cui, Y. Wang, W. Qin, H. Xu and C. Wu, *ACS Appl. Mater. Interfaces*, 2016, **8**, 3624–3634.
34 Y. Li, N. Zhang, W. W. Zhao, D. C. Jiang, J. J. Xu and H. Y. Chen, *Anal. Chem.*, 2017, **89**, 4945–4950.
35 X. M. Shi, L. P. Mei, N. Zhang, W. W. Zhao, J. J. Xu and H. Y. Chen, *Anal. Chem.*, 2018, **90**, 8300–8303.
36 X. M. Shi, L. P. Mei, Q. Wang, W. W. Zhao, J. J. Xu and H. Y. Chen, *Anal. Chem.*, 2018, **90**, 4277–4281.
37 N. Zhang, X. M. Shi, H. Q. Guo, X. Z. Zhao, W. W. Zhao, J. J. Xu and H. Y. Chen, *Anal. Chem.*, 2018, **90**, 11892–11898.
38 L. Zhang, X. M. Shi, Y. T. Xu, G. C. Fan, Y. Y. Liang, C. Wang and W. W. Zhao, *Anal. Chem.*, 2019, **91**, 6403–6407.
39 J. Wang, S. Zhang, H. Dai, H. Zheng, Z. Hong and Y. Lin, *Biosens. Bioelectron.*, 2019, **142**, 111567.
40 L. Mao, M. Gao, X. Xue, L. Yao, W. Wen, X. Zhang and S. Wang, *Anal. Chim. Acta*, 2019, **1059**, 94–102.
41 J. H. Kim, P. W. Liang, S. T. Williams, N. Cho, C. C. Chueh, M. S. Glaz, D. S. Ginger and A. K. Y. Jen, *Adv. Mater.*, 2015, **27**, 695–701.
42 B. Zhang, J. Su, X. Guo, L. Zhou, Z. Lin, L. Feng, J. Zhang, J. Chang and Y. Hao, *Adv. Sci.*, 2020, **7**, 1903044.
43 E. B. Bahadır and M. K. Sezgintürk, *Talanta*, 2016, **148**, 427–438.
44 Q. Wang, Y. F. Ruan, W. W. Zhao, P. Lin, J. J. Xu and H. Y. Chen, *Anal. Chem.*, 2018, **90**, 3759–3765.
45 G. L. Wang, F. Yuan, T. Gu, Y. Dong, Q. Wang and W. W. Zhao, *Anal. Chem.*, 2018, **90**, 1492–1497.
46 H. Liu, B. Liu, P. Huang, Y. Wu, F. Y. Wu and L. Ma, *Microchim. Acta*, 2020, **187**, 551.
47 H. Ao, Z. Qian, Y. Zhu, M. Zhao, C. Tang, Y. Huang, H. Feng and A. Wang, *Biosens. Bioelectron.*, 2016, **86**, 542–547.
48 S. Y. Yu, T. Y. Xue, L. B. Zhu, G. C. Fan, D. M. Han, C. S. Wang and W. W. Zhao, *Biosens. Bioelectron.*, 2019, **136**, 128–131.
49 X. Guo, J. Wu, L. Xia, M. Xiang, F. Qu and J. Li, *Sci. China: Chem.*, 2020, **63**, 1012–1018.